J Forensic Sci, Nov. 2005, Vol. 50, No. 6
Paper ID JFS2004547
Available online at: www.astm.org

Sven De Greef,[1] *D.D.S.; Peter Claes,*[2] *M.Sc.Eng.; Wouter Mollemans,*[2] *M.Sc.Eng.; Miet Loubele,*[2] *M.Sc.Eng.; Dirk Vandermeulen,*[2] *M.Sc.Eng., Ph.D.; Paul Suetens,*[2] *M.Sc.Eng., Ph.D.; and Guy Willems,*[1] *D.D.S., Ph.D.*

Semi-automated Ultrasound Facial Soft Tissue Depth Registration: Method and Validation*

ABSTRACT: A mobile and fast, semi-automatic ultrasound (US) system was developed for facial soft tissue depth registration. The system consists of an A-Scan ultrasound device connected to a portable PC with interfacing and controlling software. For 52 cephalometric landmarks, the system was tested for repeatability and accuracy by evaluating intra-observer agreement and comparing ultrasound and CT-scan results on 12 subjects planned for craniofacial surgery, respectively. A paired t-test evaluating repeatability of the ultrasound measurements showed 5.7% ($n = 3$) of the landmarks being significantly different ($p < 0.01$). US and CT-scan results showed significant differences ($p < 0.01$) using a Wilcoxon signed rank test analysis for 11.5% ($n = 6$) of the landmarks. This is attributed to a difference in the volunteer's head position between lying (CT) and sitting (US). Based on these tests, we conclude that the proposed registration system and measurement protocol allows relatively fast (52 landmarks/20 min), non-invasive, repeatable and accurate acquisition of facial soft tissue depth measurements.

KEYWORDS: forensic science, human anthropology, facial soft tissue depths, ultrasound, CT-scan, computer-aided

Forensic identifications are mostly based on comparisons of ante- and post-mortem data, such as medical files, dental records, X-rays or DNA. This whole procedure becomes less evident when dealing with skeletonised human remains, where any link with a possible identity is missing. In these circumstances, a cranio-facial reconstruction might help the investigation out of the impasse. Different 2D and 3D manual or computer-aided facial reconstruction techniques have been developed (1–7) for this purpose. Apart from some techniques (8–10), the majority of the reconstruction techniques use facial soft tissue depth chart data. A number of facial soft tissue depth tables have been published, measured on different biological groups, using a variety of measurement methods such as puncturing, lateral cephalometric radiographs (11–14), ultrasound (15–21), MRI and CT-scanning (22,23). Poor relationships have been reported between cadaver-based and in-vivo measurements, due to tissue deformation after post-mortem changes, such as dehydration and shrinkage or even swelling with the onset of putrefaction. The accuracy of the tissue depth data improved with the arrival of in vivo, non-invasive depth measurements. However, comparing the results of different studies became less evident due to the differences in acquisition and craniofacial landmark locations. Moreover, none of the actual studies have reported any validation results. As far as the European adult Caucasoid is concerned, it should be noticed that, although the first tissue depth registrations were performed by German anatomists at the end of the nineteenth century (1), in vivo studies were until now limited to the study of Helmer (16). Even today, the soft tissue depth charts from the cadaver study on American Caucasoids of Rhine and Moore (24) are most commonly used as guidelines in the reconstruction of adult Caucasoid faces.

The aim of the present study is to develop a user-friendly, fast, mobile and well validated measuring device to update facial soft tissue depth charts of the contemporary adult Caucasoid.

Materials and Methods

Selection of Landmarks

Similar to the study performed by Brown et al. (25), the traditional landmarks of Kolmann and Büchly (26) were compared with previous studies on adult Caucasoid (24,16) and other ultrasound studies (17–21). A total of 52 landmarks (LMs) were finally selected, 10 located on the midline and 21 located bilaterally. The selection of these landmarks was based on their presence in other studies (allowing comparisons) but also on the ability to reliably locate these landmarks in a standardised way on the face of the volunteers (Table 1, Fig. 1).

Measurement Device

In order to reach an as large as possible volunteer group and considering the pro's and con's of previous techniques, a mobile ultrasound (US) system was selected and software was developed to minimize overhead in data processing and storage.

"A-scan" as well as "B-scan" ultrasound devices have been used in former studies. Because of the complexity of the "B-scan" image data, in contrast to the simple 1D curves of the "A-scan"-device, the increased storage requirements and data transfer times as well as the bulky transducers of "B-scan"-devices, an "A-scan"-device was selected (Epoch 4b®, Panametrics, Waltham, USA). This industrial ultrasound device is compact, mobile and lightweight (2.6 kg,

[1] Katholieke Universiteit Leuven, Faculty of Medicine, School of Dentistry, Oral Pathology and Maxillofacial Surgery, Forensic Dentistry, Kapucijnenvoer 7, B-3000 Leuven, Belgium.

[2] Katholieke Universiteit Leuven, Faculty of Engineering, Medical Image Computing-ESAT/PSI, University Hospital Gasthuisberg, Herestraat 49, B-3000 Leuven, Belgium.

* This paper was presented at the AAFS 2005 57th Annual Meeting in New Orleans, LA.

Received 29 Dec. 2004; and in revised form 14 May 2005; accepted 14 May 2005; published 14 Sept. 2005.

TABLE 1—*Description of landmark location on the face.*

	Midline:	
1	Supraglabella	Most anterior point on midline
2	Glabella	Crosspoint between midline and supraorbital line
3	Nasion	Midpoint of the fronto-nasal suture
4	End of nasal	Passage between bone and cartilage of the nose
5	Mid-Philtrum	Centered between nose and mouth on midline
6	Upper lip	Midline on the upper lip
7	Lower lip	Midline on the lower lip
8	Chin-lip fold	Midline centered in fold of chin, below lips
9	Mental emminence	Centered on forward most projecting point of chin
10	Beneath chin	The vertical measure of the soft tissue on the lower edge of the chin
Left/Right	Bilateral:	
32/11	Frontal emminence	Centered on eyepupil, most anterior point of the forehead
33/12	Supraorbital	Centered on eyepupil, just above eyebrow
34/13	Lateral glabella	Junction of the frontal, maxillary, and lacrimal bones on the medial bone of the orbit
35/14	Lateral nasal	Side of the bridge of the nose, horizontal just above the end of nasal on a vertical line with the inner canthus of the eye
36/15	Suborbital	Centered on eyepupil, just under inferior orbita margin
37/16	Inferior malar	Centered on the eyepupil, midway between suborbital and lateral nostril
38/17	Lateral nostril	Next to the most lateral point of the ala nasi
39/18	Naso-labial ridge	The prominence next to the mid-philtrum
40/19	Supra canina	Vertically lined up with the cheilion, on the horizontal level of the Mid-philtrum
41/20	Sub canina	Vertically lined up with the cheilion, on the horizontal level of the Chin-lip fold
42/21	Mental tubercle anterior	Most prominent point on the lateral bulge of the chin mound
43/22	Mid lateral orbit	Vertically centered on the orbit, next to the lateral orbit border
44/23	Supraglenoid	Root of the zygomatic arch just before the ear
45/24	Zygomatic arch	Maximum, most lateral curvature of the zygomatic bone
46/25	Lateral orbit	Lined up with the lateral border of the eye on the center of the zygomatic process
47/26	Supra M2	Cheek region, lateral—lined up with bottom of nose; vertical—lined up beneath lateral border of the eye
48/27	Mid masseter	Middle of the masseter, the halfway point between the supraglenoid and the gonion
49/28	Occlusal line	Border of the masseter, on vertical level of the cheilion
50/29	Sub M2	Below the second molar on horizontally lined up with supra M2
51/30	Gonion	At the angle of the mandible
52/31	Mid mandibular	Inferior border of the mandible, vertically lined up with supra M2

battery included) (Fig. 2). A flat and small (6 mm diameter), 10 MHz ultrasound transducer is used for accurately pointing to and analyzing the landmarks. Furthermore, this device has a serial (RS-232) communication port, for connection with a PC.

Control Software

A Matlab-based (The Mathworks Inc., Natick, MA) interface program was created to speed up the registration process by partially automating data transfer and device setup. Except for the input of specific properties of the volunteers and positioning of the transducer on the landmarks, the whole process is controlled using a 3-button wireless infrared mouse. Mouse clicks control the following tasks: (1) freezing or unfreezing the A-scan curve; (2) transferring the curve from the ultrasound device to the PC, where the curve and the automatically calculated associated tissue depth are stored in the database; and (3) proceeding to the next landmark with automatic changing of the device settings. The tissue depths are determined from the A-scan curve as the horizontal position (distance to US transducer) corresponding to the maximal peak within a predefined interval on the curve, called the gate. The settings of the Epoch 4b® include the magnification of the measured ultrasound signal (the gain), the distance interval over which it is measured (the range) and the maximum peak detection window (the gate). These settings were originally based on the results of former soft tissue depth studies and refined after a training period with the "A-scan"-device.

Database Management

In order to easily extract specific data and perform statistical analysis, we created a database using MySQL software (MySQL AB, Uppsala, Sweden). The database is composed of 5 tables. One table contains all the personal information of the volunteer: name, birth date, health status, weight, length, facial profile, presence of dental prosthesis, plastic surgery, ethnic background, registration date and space for extra comments. A second table contains 36 different categories based on sex (M/F), age (18–35y, 35–50y, 50+), body mass index (−25, +25) and facial profile (concave, convex, straight). A third table contains the 52 landmarks of the face. Based on the volunteer's category and the landmark to measure, the interface program retrieves the necessary information, out of a fourth "settings" table, for the automatic adjustment of the Epoch4b® such as the range, gain and detection gate. Finally, in the fifth table, all the measurement results and corresponding curves are stored.

Registration Protocol

The registration procedure starts by entering the volunteer's identity and physical properties in the computer. The patient is measured in an upright relaxed position. With the probe as perpendicular as possible to the underlying bone and using a classic neutral coupling echogel, tissue depth is measured taking care not to indent the facial soft tissues. The correct transducer position is obtained by first compressing and depressing the tissues in order to differentiate the noise from the genuine US reflections. Secondly, the transducer orientation is interactively determined such that the highest peak, corresponding to the most perpendicular position of the transducer to the bone, is obtained. Finally, the compression on the soft tissue is maximally reduced avoiding losing skin contact. This technique was first practised on (fresh) corpses in combination with needle puncturing. Three measurements are obtained, the highest of which

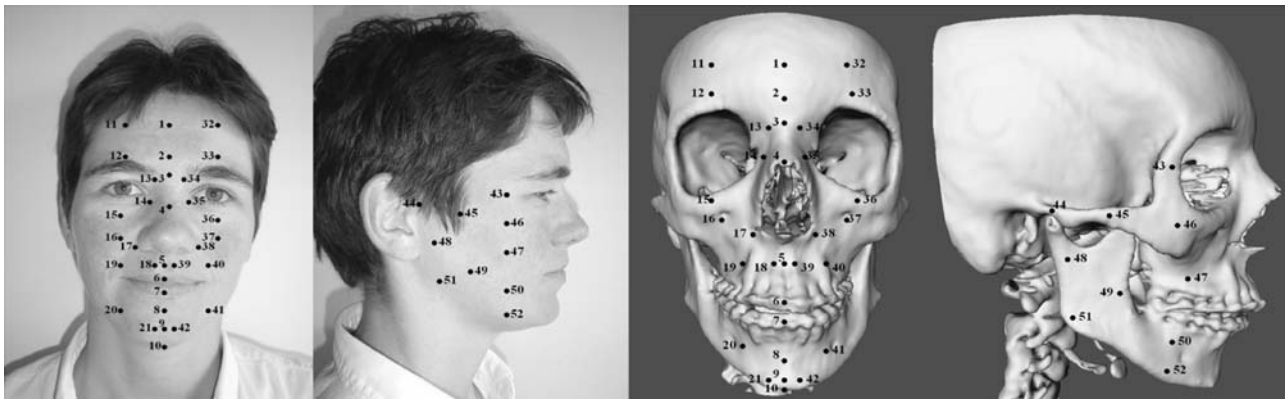

FIG. 1—*Landmark locations on the face and the skull in frontal and lateral view.*

FIG. 2—*The Epoch 4b® ultrasound device.*

FIG. 3—*The system set-up.*

is taken into account for further statistics. As mentioned before, except for the correct positioning of the transducer, the data treatment occurs automatically using the mouse clicks (Fig. 3).

Validation: Repeatability and Accuracy

For the repeatability evaluation of the US measurements a test group of 33 volunteers, composed of 19 males and 14 females with average age 39.0 years (s.d. 17 years) and average BMI 26.5 (s.d. 6.46), was measured twice (US1, US2), with time intervals varying between 2 days and 2 months. Accuracy was tested comparing ultrasound with CT-scan results. Twelve patients (11 females and 1 male with average age 19.7 years and average BMI 19.5) consented to have their facial soft tissue depths ultrasonically registered (US) before acquisition of a total head CT-scan for preoperative osteotomy planning. Prior to the ultrasound registration, the 52 landmarks were marked on the face using a blue eyeliner pencil and a 3D picture of the face was taken using a 3D portable camera (ShapeCam, Eyetronics, Leuven, Belgium). The skull surface (Fig. 4*a*) and external surface of the skin (Fig. 4*b*) were extracted from the CT images by simple thresholding of the CT values (at a Hounsfield Unit value of 300 and −400, resp.). The extracted surfaces are represented at sub-voxel precision as a mesh of triangular tiles using standard surface meshing software (27). The 3D facial surface obtained with the 3D camera was automatically fitted to the CT-based skin surface (minimizing the distance between the two surfaces using the method presented in (28)). This allows texturing of the CT extracted skin surface with the texture obtained from the 3D picture (Fig. 4*c*) in order to determine the CT-coordinates of the exact landmark locations as measured with ultrasound. A software program was developed to perform virtual "A-scan" ultrasonography (Fig. 4*d*), allowing to measure the CT-based soft tissue depths at the 52 different landmarks locations as indicated by the blue points prior to ultrasound registration. The virtual US probe is manually positioned on a 3D graphical rendering of the textured CT skin surface at each skin-based landmark location. The algorithm then iteratively estimates the corresponding skull base point at which the normal to the skull surface is as parallel as possible to the transducer orientation at the skin landmark. This mimics the real ultrasound measuring protocol as closely as possible. The distance between the skin landmark and corresponding skull base point is stored as the associated CT soft tissue depth.

Finally, in order to examine the influence of gravity on the differences in tissue depths as measured by CT and ultrasound, the external skin surface extracted from CT, measured in supine position, was aligned for each individual with the 3D facial surface obtained by the 3D camera in upright position. In order to limit the influence of expected differences, the surface alignment is only based on corresponding surface parts that are less than a maximal (2 mm) distance apart.

Statistical Analysis

The intra-observer agreement was statistically analysed with a paired t-test and a Wilcoxon paired Signed Rank test. The latter

FIG. 4—*Skull (a) and skin (b) surface segmented from CT scan image data. Textured skin surface (c) and virtual ultrasonography view (d).*

procedure tests for the null-hypothesis of the median of the paired differences to be zero. The accuracy of US measurements compared to CT-based measurements was statistically analysed using the Wilcoxon paired Signed Rank test. Given the limited ($n = 12$) number of observations, this non-parametric test was preferred over the simpler paired t-test since it has a higher power efficiency (higher sensitivity for smaller sample sizes) and higher robustness to violations of the normality assumptions. Confidence intervals for the median of the differences were calculated for each landmark using a bootstrapping technique (resampling with replacement (29)). Bland-Altman graphs are constructed for selected landmarks to picture the relationship between differences, average values and confidence limits (30). A robust linear regression (31) between CT and ultrasound measurements was calculated to look for any linear bias (offset and/or slope) due to either ultrasound miscalibration (time-to-distance transformation based on estimated sound velocity in soft tissue) or CT distance offsets (incorrect segmentation thresholds). All tests were implemented using the Matlab 6R13 (The Mathworks Inc., Natick, MA) data analysis software.

Results

Intra-observer Repeatability

The paired differences (US1 minus US2) for the ultrasound repeatability study showed a mean of 0.09 mm and standard deviation (sd) of 2.17 mm, grouped over all landmarks. A normal probability plot indicated a light-tailed deviation from the normal probability at the extremes. Both the paired t-test and the Wilcoxon paired signed rank test (Table 2A), applied to each landmark separately, showed only 5.8% ($n = 3$) of the landmarks to have a significant difference ($p < 0.01$) between the two runs. These apparently very simple landmarks are the left (LM 33) and right supra-orbital (LM 12) and the left frontal (LM 32) eminence. These findings are also confirmed by the 99% confidence intervals for the median of the differences as calculated using the bootstrapping procedure (Fig. 5). Note that, if the zero value lies outside the confidence interval, the null-hypothesis of no difference can be rejected at the associated significance level. A Bland-Altman graph, plotting the pairwise differences versus the pairwise means, is shown in Fig. 6. None of the three statistical tests showed any significant left versus right differences (both time points grouped) at the $p < 0.01$ significance level.

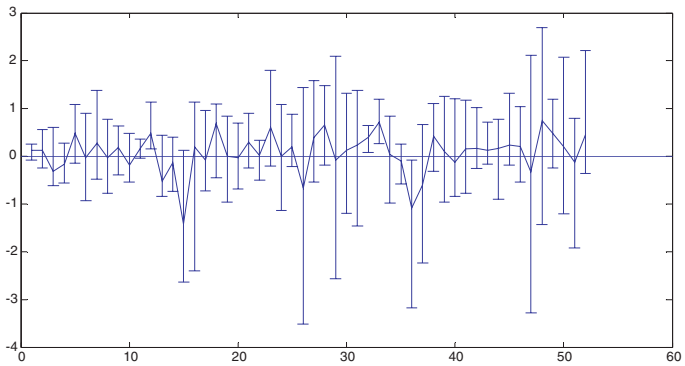

FIG. 5—*Median and 99% confidence intervals (in mm) for the median of the difference US1–US2 for each landmark. Landmark numbering along horizontal axis.*

Accuracy Compared to CT

Six of the 52 landmarks (Table 2B) showed a statistical difference between the ultrasound (US) and CT measurements using the Wilcoxon paired signed rank test at a significance level $p < 0.01$. These landmarks are, bilaterally, the mid-masseter (LM 27,48) and occlusal line (LM 28,49) and the right gonion (LM 30) and right supraglenoid (LM 23). The bootstrap-based 99% confidence intervals for the median (Fig. 7) indicate the same set of landmarks as being different. The Bland-Altman graph for these landmarks is shown in Fig. 8. A robust linear regression estimation of CT versus US (CT = a.US + b), grouped over all landmarks returns a value for the slope a = 1.01 and the intercept b = 0.23.

Supine Versus Upright Comparison

Table 2C lists, for each landmark, the median (over all subjects) signed distances between the CT-based skin surface and the 3D

TABLE 2—*Statistical results for repeatability (A), accuracy (B) and difference supine versus upright (C). ($p < 0.05$ (*), $p < 0.01$ (**) and $p < 0.001$ (***)).*

		A Median (US1–US2)	B Median (CT–US)	C Median (CT–3D)
	Midline:			
1	Supraglabella	0.12	−0.20	−0.04
2	Glabella	0.12	0.04	0.16
3	Nasion	−0.32	0.10	0.26
4	End of Nasals	−0.16	−0.66*	0.64
5	Mid-Philtrum	0.48	−0.34	0.23
6	Upper lip Margin	−0.03	−0.16	−0.02
7	Lower lip Margin	0.28	0.04	−0.13
8	Chin-lip fold	−0.03	0.97*	0.08
9	Mental emminence	0.18	−0.14	−0.58
10	Beneath chin	−0.18	1.05	0.69
	Bilateral:			
11	Frontal emminence	0.16*	−0.16	0.18
12	Supraorbital	0.48***	−0.06	−0.17
13	Lateral glabella	−0.52	0.28	0.16
14	Lateral nasal	−0.13	−0.28	−0.26
15	Suborbital	−1.42*	−0.60	0.31
16	Inferior malar	0.20	−1.13*	−0.79
17	Lateral nostril	−0.08	0.19	−0.64
18	Naso-labial ridge	0.69	0.71	0.44
19	Supra canina	0	1.405*	−0.60
20	Sub canina	−0.03	−0.14	−0.48
21	Mental tubercle anterior	0.30*	0.56	−0.39
22	Mid lateral orbit	0.02	−0.59	−0.55
23	Supraglenoid	0.60	2.03**	−0.76
24	Zygomatic arch	0	0.52	−0.03
25	Lateral orbit	0.20	−0.60	0.31
26	Supra M2	−0.66	0.56	0.47
27	Mid masseter	0.39	1.50**	1.99
28	Occlusal line	0.66*	2.82***	1.59
29	Sub M2	−0.08	0.99	−1.50
30	Gonion	0.12	2.71**	1.54
31	Mid mandibular	0.24	−0.35	−0.53
32	Frontal emminence	0.40***	−0.20	−0.21
33	Supraorbital	0.72***	0.004	0.04
34	Lateral glabella	0.04	−0.001	0.24
35	Lateral nasal	−0.10	−0.67*	0.38
36	Suborbital	−1.08	−1.03	0.37
37	Inferior malar	−0.60	−0.19	−1.32
38	Lateral nostril	0.42*	0.21	−0.63
39	Naso-labial ridge	0.11	0.66*	0.20
40	Supra canina	−0.12	−0.26	−0.64
41	Sub canina	0.15	0.34	−0.31
42	Mental tubercle anterior	0.16	0.13	−0.56
43	Mid lateral orbit	0.12	−0.09	−0.44
44	Supraglenoid	0.16	1.73*	−0.11
45	Zygomatic arch	0.24	1.02*	1.09
46	Lateral orbit	0.21	0.49	0.35
47	Supra M2	−0.33	0.42	0.39
48	Mid masseter	0.75	2.78***	2.38
49	Occlusal line	0.48	3.81***	1.44
50	Sub M2	0.21	0.50	−1.50
51	Gonion	−0.12	1.41*	1.26
52	Mid mandibular	0.45	−0.08	−0.70

skin surface as acquired just prior to US registration. Figure 9 shows the absolute differences at all positions on the face for a single individual.

The median (over all subjects) soft tissue depth differences (CT minus US) at each landmark as well as the median signed distances (CT minus 3D) at each landmark are plotted in Fig. 10. A negative (positive, resp.) signed distance refers to the 3D camera skin surface being in front of (behind, resp.) the CT skin surface after alignment.

Possible linear correlations between the soft tissue depth differences (CT minus US) and the signed distances (CT minus 3D) were examined with the standard Pearson's correlation coefficient and the non-parametric Spearman rank correlation. Both correlation measures returned a value $r = 0.22$ when all measurements were paired per landmark and per subject, and a value $r = 0.53$ for the median (over all subjects) differences and median signed distances.

Discussion

The repeatability study shows very few ($n = 3$) landmarks with a statistically significant ($p < 0.01$) difference between the repeated runs. A closer look at the protocol application during this first stage of the project indicated that a slight change of transducer position had occurred between the first and second measurements. Indeed, the position of the supra-orbitalis landmark changed from "on the eyebrow" to "just above it" because of the eyebrow interference. This probably explains the significant differences for LMs 12 and 33. Furthermore, the median difference for LM 32 is very small (<0.5 mm) compared to the corresponding average thickness (4.6 mm).

The slope coefficient ($a = 1.01$) of the linear regression between CT and US measures, is very close to 1. Any miscalibration of the ultrasound device, by an improper setting of the sound velocity (set at 1542 m/s) in the measured soft tissue, would result in a value substantially different from one. We can thus conclude that this setting is accurate enough, relative to the CT standard used. The intercept value ($b = 0.23$) is close to zero. Any improper setting of the thresholds used for defining the external skin and skull surfaces in the CT images, would result in a constant offset relative to the US measures. Since the CT images were acquired and processed with typical voxel dimensions of 0.5 mm × 0.5 mm in-plane and 0.9 mm transaxially, we can conclude that the thresholds chosen are sub-voxel precise, on average.

Careful examination of the Bland-Altman graphs for all landmarks shows a small subset of clear outliers both for CT and US based measures. However, upon visual inspection of these graphs, no clear preference in any direction (positive or negative) or type (CT or US) could be observed. Note that these outlier values do not influence the results drawn by the Wilcoxon paired signed rank test, which is known to be robust to outliers. Their existence, however, requires robust statistics to be used when further processing the database. One practical consequence of this finding is that, during acquisition of the US data, a left-right check on the values obtained is calculated and the operator is given the opportunity to reregister certain landmarks signalled to be outside an acceptable left-right difference range (<3 mm).

Since landmarks found to be statistically different between CT and US were all located in the masseter region, we examined whether the differences could be explained by the influence of gravity on the soft tissue thicknesses between the upright position during the US acquisition and the supine position in the CT-scan. Figure 9 shows the typical pattern as observed for an individual case. A zero-difference (dark) band running over the naso-labial sulcus can be observed. When inspecting the aligned CT and 3D skin surface, the thickness of the regions in front of this zero-band seems to decrease from 3D to CT whereas the opposite effect occurs for the region behind.

Although a relatively weak ($r = 0.22$) linear correlation could be found between the (CT versus US) errors in the landmarks and the (3D minus CT) distances between the skin surfaces in the upright and supine position, paired per landmark and per subject, a more pronounced linear correlation ($r = 0.53$) could be established between the median differences and distances. This correlation is

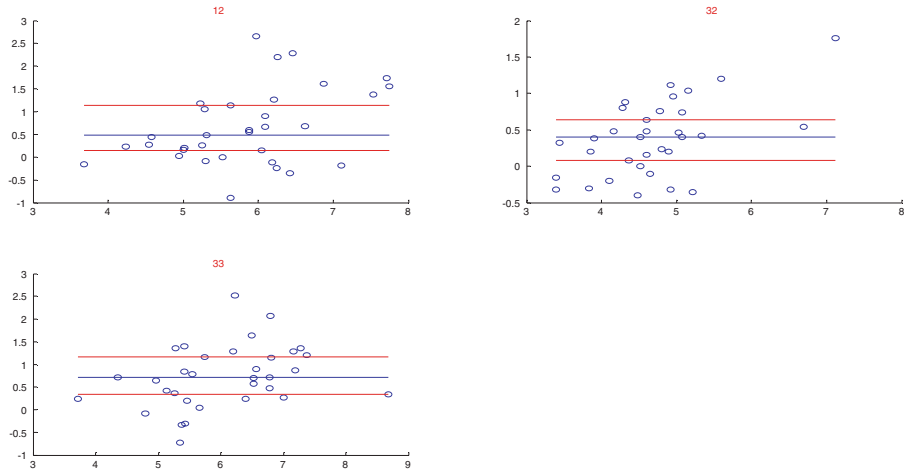

FIG. 6—*Bland-Altman graph of the pairwise differences versus their means (all in mm) for the landmarks being detected as significantly different ($p < 0.01$) between two runs of ultrasound measures. The midline is the median, the two borderlines represent the 99% confidence interval limits.*

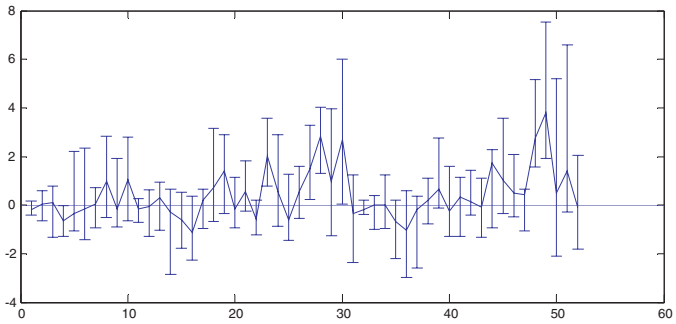

FIG. 7—*Median and 99% confidence intervals (in mm) for the median of the difference CT–US for each landmark. Landmark numbering along horizontal axis.*

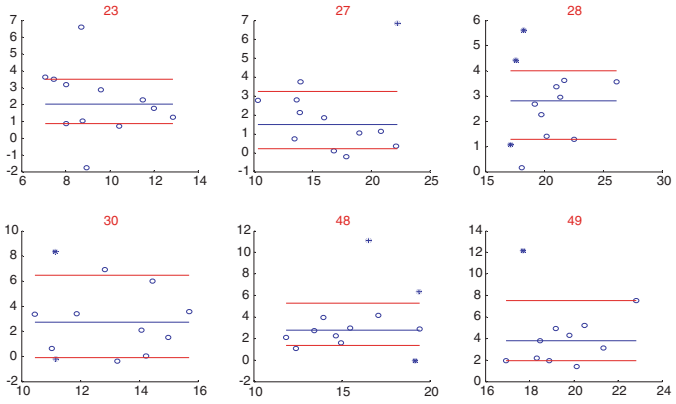

FIG. 8—*Bland-Altman graph of the pairwise differences (CT–US) versus their means (all in mm) for the landmarks being detected as significantly different ($p < 0.01$) between CT-based and US-based measures. The midline is the median, the two borderlines represent the 99% confidence interval limts. Crosses indicate CT outliers, asterisks indicate US outliers.*

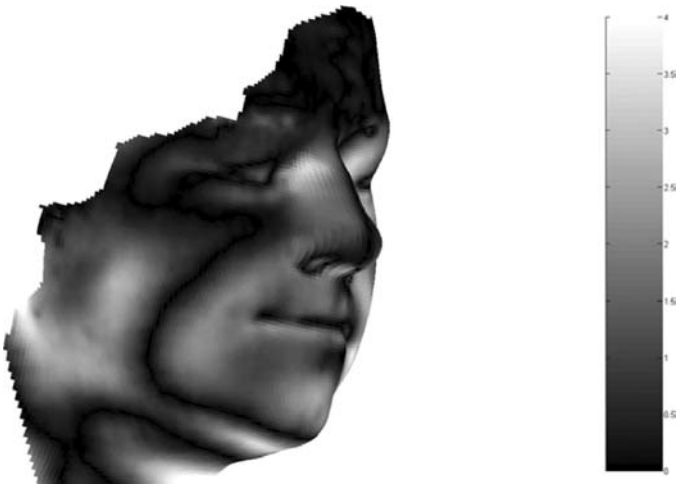

FIG. 9—*Absolute distances between 3D skin surface prior to US acquisition (upright position) and 3D skin surface extracted from CT image data (in supine position). The distances are shown here for one particular subject.*

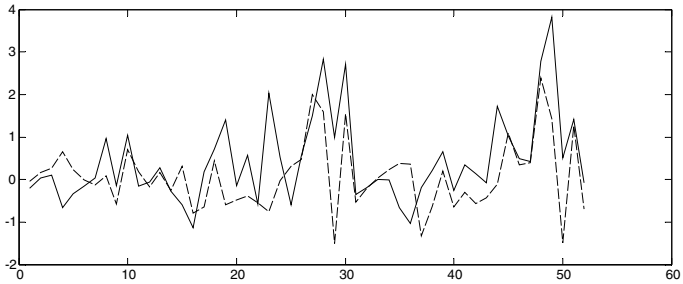

FIG. 10—*(CT minus US) median differences (bold) and signed distances (dashed) between CT-based skin surface and 3D camera skin surface (positive values are associated to 3D camera skin surface behind the CT-based surface). Values (in mm) ranked per landmark.*

visualized in Fig. 10 where we also see that the larger (CT minus US) differences and (3D minus CT) distances are located precisely at the landmarks in the gonion-, supraglenoid-, and occlusal line region, substantiating the hypothesis that they are probably due to the gravity effect.

Conclusion

Thanks to the progress in computer science and medical imaging technology it was possible to create a fast, mobile and user-friendly facial soft tissue depth acquisition system. Statistical analysis of the repeatability and accuracy proved our system to be a reliable

and accurate measurement tool. A correct application of the protocol allows in 20 min the measurement of 52 facial landmarks in a non-invasive, standardized and repeatable way. It will allow (re)evaluation of older facial soft tissue depth data based on a large group of subjects of different age, sex, race and build. An evaluation that shouldn't be limited to the facial soft tissue depth data but, as the actual tendency, expanded to other facial features in order to increase the degree of accuracy of the facial reconstruction.

Acknowledgments

This work is supported by the Flemish Institute for the Promotion of Innovation by Science and Technology in Flanders (IWT, project IWT/GBOU/020195). The authors also acknowledge the support of Dr. Nadjmi (Eeuwfeest clinic, Antwerpen, Belgium) in providing the CT data.

References

1. Aulsebrook WA, Iscan MY, Slabbert JH, Becker P. Superimposition and reconstruction in forensic facial identification: a survey. Forensic Sci Int 1995;75(2–3):101–20. [PubMed]
2. Tyrell AJ, Evison MP, Chamberlain AT, Green MA. Forensic three-dimensional facial reconstruction: historical review and contemporary developments. J Forensic Sci 1997;42(4):653–61. [PubMed]
3. Clement JG, Ranson DL, editors. Craniofacial identification in forensic medicine. London: Arnold, 1998.
4. Stoney MC, Koelmeyer TD. Facial reconstruction: a case report and review of development of techniques. Med Sci Law 1999;39(1):49–60. [PubMed]
5. Vanezis M, Vanezis P. Cranio-facial reconstruction in forensic identification—historical development and a review of current practise. Med Sci Law 2000;40(3):197–205. [PubMed]
6. Taylor KT. Forensic art and illustration. Boca Raton: CRC Press, 2001.
7. De Greef S, Willems G. Three-dimensional cranio-facial reconstruction in forensic identification: latest progress and new tendencies in the 21st century. J Forensic Sci 2005;50(1):12–17. [PubMed]
8. Gerasimov M. The face finder. Philadelphia, PA: JB Lippencott Co, 1971.
9. Quatrehomme G, Cotin S, Subsol G, Delingette H, Garidel Y, Grévin G et al. A fully three-dimensional method for facial reconstruction based on deformable models. J Forensic Sci 1997;42(4):649–52. [PubMed]
10. Nelson LA, Michael SD. The application of volume deformation to three-dimensional facial reconstruction: a comparison with previous techniques. Forensic Sci Int 1998;94(3):167–81. [PubMed]
11. Dumont ER. Mid-facial tissue depth of white children: An aid in facial feature reconstruction. J Forensic Sci 1986;31(4):1463–9. [PubMed]
12. Garlie TN, Saunders SR. Midline facial tissue thicknesses of subadults from longitudinal radiographic study. J Forensic Sci 1999;44(1):61–7. [PubMed]
13. Smith SL, Buschang PH. Midsagittal facial thicknesses of children and adolescents from the Montreal growth study. J Forensic Sci 2001;46(6):1294–302. [PubMed]
14. Williamson MA, Nawrocki SP, Rathburn TA. Variation in midfacial tissue thickness of African-american children. J Forensic Sci 2002;47(1):25–31. [PubMed]
15. Lebedinskaya GV, Stepia VS, Surinina TS, Fedosyutkin BA, Tscherbin LA. The first experience of application of ultrasound for the studies of the thickness of soft facial tissues. Soviet Ethnogr 1979;4:121–131 (in Russian). Cited in Ref. (1)
16. Helmer R. Schädelidentifizierung durch elektronische bildmischung. Heidelberg: Kriminalistik Verlag GmbH, 1984.
17. Hodson G, Lieberman LS, Wright P. In vivo measurements of facial tissue thicknesses in American Caucasoid Children. J Forensic Sci 1985;30(4):1100–12. [PubMed]
18. Aulsebrook WA, Becker PJ, Iscan MY. Facial soft-tissue thicknesses in the adult male Zulu. Forensic Sci Int 1996;79(2):83–102. [PubMed]
19. Manhein MH, Listi GA, Barsley RE, Musselman R, Barrow NE, Ubelbaker DH. In vivo facial tissue depth measurements for children and adults. J Forensic Sci 2000;45(1):48–60. [PubMed]
20. El-Mehallawi IH, Soliman EM. Ultrasonic assessment of facial soft tissue thicknesses in adult Egyptians. Forensic Sci Int 2001;117(1–2):99–107. [PubMed]
21. Wilkinson CM. In vivo facial tissue depth measurements for White Britsh children. J Forensic Sci 2002;47(3):459–65. [PubMed]
22. Phillips VM, Smuts NA. Facial reconstruction: utilization of computerized tomography to measure facial tissue thickness in a mixed racial population. Forensic Sci Int 1996;83(1):51–9. [PubMed]
23. Vignal JN, Schuliar Y. Computer-assisted facial reconstruction. Three years' results and new perspectives. Proceedings of the Tenth Meeting of the International Association for Craniofacial Identification; 2002 Sep 11–14; Bari Italy. Bari: Università degli Studi di Bari, 2002.
24. Rhine JS, Moore CE. Tables of facial tissue thickness of American Caucasoids in forensic anthropology. Maxwell Museum Technical series 1984;1. Cited in (6).
25. Brown RE, Kelliher TP, Tu PH, Turner WD, Taister MA, Miller KWP. A survey of tissue-depth landmarks for facial approximation. Forensic Sci Communications 2004;6(1).
26. Kollmann J, Buchly W. Die persistenz der rassen und die reconstruction der physiognomie prahistorischer schadel. Archiv fur anthropologie 1898;25:329–59. Cited in (6).
27. Lorensen B, Cline HE. Marching Cubes: A high resolution 3d surface construction algorithm. Computer Graphics (Proceedings of Siggraph 1987) 1987;21:163–9.
28. Claes P, Vandermeulen D, Van Gool L, Suetens P. Automatic, robust and accurate 3D modelling based on variational implicit surfaces. Technical Report KUL/ESAT/PSI/0405 2004: available at www.medicalimagecomputing.com/publications.
29. Good PI. Resampling methods: a practical guide to data analysis. Boston: Birkhäuser, 1999.
30. Altman DG, Bland JM. Measurement in medicine: the analysis of method comparison studies. The Statistician 1983;32:307–17.
31. Holland PW, Welsch RE. Robust regression using iteratively reweighted least-squares. Communications in statistics: theory and methods 1977;A6:813–27.

Additional information and reprint requests:
Prof. Guy Willems, Ph.D.
Katholieke Universiteit Leuven
Faculty of Medicine
School of Dentistry, Oral Pathology and Maxillofacial Surgery
Forensic Dentistry
Kapucijnenvoer 7
B-3000 Leuven
Belgium
E-mail: Guy.willems@med.kuleuven.ac.be